





Single pair of charge-2 high-fold fermions with surface type-II Van Hove singularities in ultralight chiral crystals

Xiaoliang Xiao ¹, Yuanjun Jin ², Da-Shuai Ma,^{1,3} Haoran Wei ¹, Jing Fan ⁴, Rui Wang,^{1,3,5} and Xiaozhi Wu^{1,5,*}

¹*Institute for Structure and Function & Department of Physics, Chongqing University, Chongqing 400044, China*

²*Guangdong Basic Research Center of Excellence for Structure and Fundamental Interactions of Matter, Guangdong Provincial Key Laboratory of Quantum Engineering and Quantum Materials, School of Physics, South China Normal University, Guangzhou 510006, China*

³*Center of Quantum Materials and Devices, Chongqing University, Chongqing 400044, China*

⁴*Center for Computational Science and Engineering, Southern University of Science and Technology, Shenzhen 518055, China*

⁵*Chongqing Key Laboratory for Strongly Coupled Physics, Chongqing 400044, China*



(Received 13 December 2023; revised 29 January 2024; accepted 4 April 2024; published 19 April 2024)

The realization of the single-pair fermions in electronic systems remains challenging in topology physics, especially for the systems with larger chiral charges C . In this work, based on the symmetry analysis, low-energy effective models, and first-principles calculations, we identify the single-pair charge-two chiral fermions in cubic lattices. We first derive the minimal lattice model that exhibits a single pair of Weyl points with the opposite chiral charges of $C = \pm 2$. Furthermore, we show the ultralight chiral crystal $P4_332$ -type LiC_2 and its mirror enantiomer as high-quality candidate materials, which exhibit large energy windows to surmount the interruption of irrelevant bands. Since two enantiomers are connected by the mirror symmetry, we observe the opposite chiral charges C and the reversal of Fermi-arc connections, showing the correspondence of chirality in the momentum space and the real space. In addition, we also reveal type-II van Hove singularities on the helicoid surfaces, which may induce chirality-locked charge density waves on the crystal surface. Our work not only provides a promising platform for controlling the sign of chiral charge through structural chirality but also facilitates the exploration of electronic correlations on the surface of ultralight chiral crystals.

DOI: [10.1103/PhysRevB.109.165136](https://doi.org/10.1103/PhysRevB.109.165136)

I. INTRODUCTION

The classification of the band topology, by the crystallographic space group (SG) symmetry, can give rise to distinct types of unconventional chiral Weyl fermions (CWFs) [1–6], which are usually characterized by larger chiral charges C or higher degeneracies at crossing points. To date, they roughly contain twofold quadratic (cubic and quadruple) Weyl fermions with $C = \pm 2$ (± 3 and ± 4) [2,7–13], threefold charge-two (C-2) spin-1 Weyl fermions [1,14] [see Fig. 1(a)], fourfold C-2 Dirac and C-4 spin- $\frac{3}{2}$ Weyl fermions [1,3,4,15] [see Figs. 1(b) and 1(c)], sixfold C-4 double spin-1 Weyl fermions [1] [see Fig. 1(d)], and so on [6]. The chiral crystal [16], lacking the inversion, mirror, and rotoinversion symmetry, is regarded as a natural platform for achieving these CWFs in condensed matter physics. Besides, exploring these unconventional CWFs in chiral crystals can provide a new perspective for discovering interesting physical properties, such as longer Fermi arc surface states [17–23], larger quantized circular photogalvanic effect [24–26], etc. [27–30].

The systems with the single-pair Weyl points (WPs) have attracted considerable attention [17,19,31–38] since the simple Fermi-arc connections of WPs make their topological surface state (TSSs) easy to be imaged in spectroscopy experiments [20–22,39]. Among them, the $P2_13$ -type materials with

$SG P2_13$ [No. 198], including the XSi ($X = \text{Co}, \text{Rh}$) family and PdGa crystals, have been experimentally identified to own a pair of C-4 WPs [17–23,39–41]. Interestingly, on the (001) surface of XSi crystals, type-II van Hove singularities (VHSs), where the Lifshitz transitions occur at a generic momentum \mathbf{k} , and chirality-locked charge density waves (CDW) were observed to manifest at the helicoid surface states [42–44]. This discovery makes it possible to study interaction-driven order states on the surface of topological materials [45,46]. However, the $P2_13$ -type materials carry chiral charges of $C = \pm 4$ but $C = \pm 2$. Due to the non-negligible spin-orbit coupling (SOC) effect, the threefold C-2 spin-1 WP (SWP) and fourfold C-2 Dirac point (DP) are driven into the fourfold C-4 spin- $\frac{3}{2}$ WP and sixfold C-4 double SWP, respectively, resulting in a single pair of C-4 CWFs [17,19,47,48]. Therefore, the single-pair C-2 WPs have so far mainly been realized in bosonic and artificial systems without the known SOC mechanisms [49–53], but very rarely in electronic systems [14]. Fortunately, there is a class of ultralight materials composed of light atoms with negligible SOC in nature. In fact, the study of topological states in ultralight materials is quite important in fermionic systems, and the prime examples of which are the Dirac fermions in graphene [54], etc. [13,15,55–62]. Hence, these ultralight materials provide a promising platform to search for a class of candidates that permit the single-pair high-fold C-2 CWFs.

In this work, based on symmetry arguments and the low-energy effective model, we identify that the single-pair

*xiaozhiwu@cqu.edu.cn

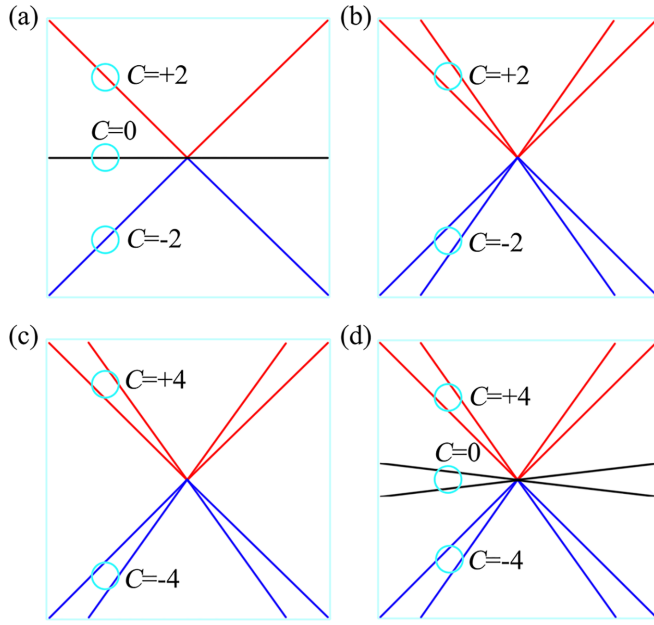


FIG. 1. Four types of unconventional chiral fermions with the high-fold degeneracy. (a) Threefold spin-1 Weyl fermions. (b) Fourfold charge-2 Dirac fermions, which are equivalent to adding two spin- $\frac{1}{2}$ Weyl fermions with the same chirality. (c) Fourfold spin- $\frac{3}{2}$ Weyl fermions. (d) Sixfold double spin-1 Weyl fermions, which are a composition of two identical spin-1 Weyl fermions. The bands marked the corresponding chiral charges, respectively.

high-fold CWFs with chiral charges of $C = \pm 2$ can exist in chiral cubic crystals. We further construct the minimal lattice model, which captures all the topological properties and generates visible double-helicoid Fermi arcs spanning the entire (001) surface Brillouin zone (BZ). Furthermore, by first-principles calculations, we take the ultralight crystal LiC_2 crystallized in SG $P4_332$, called $P4_332$ -type LiC_2 , and its mirror enantiomer as concrete examples to confirm the single-pair high-fold CWFs. Compared to previously reported $P2_13$ -type materials, our materials have three distinctions: (i) The SOC effect is indeed pretty small. (ii) The C-2 DP of the R point in the two enantiomers is described by a corepresentation equivalent to a four-dimensional (4D) single-valued irreducible representation (SVIR), but the DP in $P2_13$ -type materials is described by the time-reversal (\mathcal{T}) symmetric corepresentation formed by pairing two two-dimensional (2D) SVIRs. (iii) $P4_332$ -type LiC_2 possess the mirror enantiomer $P4_132$ -type LiC_2 with different SG. Besides, $P4_332$ -type LiC_2 is an ideal semimetal with clear high-fold fermions near the Fermi level, unlike $P2_13$ -type PdGa enantiomers which are involved trivial bands and whose chiral fermions are far away from the Fermi level [40]. Moreover, the two enantiomers with opposite chiral charges C exhibit the reversal of Fermi-arc connections. Our work provides an ideal platform to explore the single-pair high-fold WPs with $C = \pm 2$ and control the sign of chiral charges by the handedness of chiral crystals. Finally, we unveil type-II VHSs on the (001) surface of $P4_332$ -type LiC_2 , offering a promising platform to explore electronic correlated phenomena such as chirality-locked CDW, unconventional superconductivity, and more.

TABLE I. Three chiral SGs hosting the single-pair high-fold C-2 CWFs (i.e., SWP and C-2 DP) with negligible SOC effect. Location is the high-symmetry momentum \mathbf{k} . Type is the types of WPs. Generators denote the point-group parts of the generators of the little group at \mathbf{k} .

SG	Location	Type	Generators
$P2_13$	$\Gamma: (0, 0, 0)$	SWP	$\tilde{C}_{3,111}^+, \tilde{C}_{2x}, \tilde{C}_{2y}, \mathcal{T}$
	$R: (\frac{1}{2}, \frac{1}{2}, \frac{1}{2})$	C-2 DP	$\tilde{C}_{3,111}^+, \tilde{C}_{2x}, \tilde{C}_{2y}, \mathcal{T}$
$P4_332$	$\Gamma: (0, 0, 0)$	SWP	$\tilde{C}_{3,111}^+, \tilde{C}_{4z}, \tilde{C}_{2x}, \tilde{C}_{2y}, \mathcal{T}$
	$R: (\frac{1}{2}, \frac{1}{2}, \frac{1}{2})$	C-2 DP	$\tilde{C}_{3,111}^+, \tilde{C}_{4z}, \tilde{C}_{2x}, \tilde{C}_{2y}, \mathcal{T}$
$P4_132$	$\Gamma: (0, 0, 0)$	SWP	$\tilde{C}_{3,111}^+, \tilde{C}_{4z}, \tilde{C}_{2x}, \tilde{C}_{2y}, \mathcal{T}$
	$R: (\frac{1}{2}, \frac{1}{2}, \frac{1}{2})$	C-2 DP	$\tilde{C}_{3,111}^+, \tilde{C}_{4z}, \tilde{C}_{2x}, \tilde{C}_{2y}, \mathcal{T}$

II. SYMMETRY ARGUMENTS AND MINIMAL LATTICE MODEL

First, we begin analyzing the symmetry conditions to search for a single pair of CWFs with the coexistence of SWP and C-2 DP in spinless systems. The symmetry argument goes as follows. For nonmagnetic systems with single-pair WPs, their WPs must be located at the time-reversal-invariant momentum points [31,63,64]. Hence, only time-reversal-invariant high-symmetry points (HSPs) are considered. First of all, considering the C-2 DP, the band crossing \mathbf{k} point should possess two 2D SVIRs or a 4D SVIR [65]. By scanning through all the SVIRs of the little group at these HSPs for 230 SGs [65], six SGs can be found, i.e., No. 19 (R), No. 92(A), No. 96 (A), No. 198 (R), No. 212 (R), and No. 213 (R). Here, it can be discovered that the minimal SG of the C-2 DP is SG 19 with two screw rotational symmetries ($\tilde{C}_{2x} = \{C_{2x} | \frac{1}{2} \frac{1}{2} 0\}$ and $\tilde{C}_{2y} = \{C_{2y} | 0 \frac{1}{2} \frac{1}{2}\}$) and \mathcal{T} symmetry. Among six SGs, three SGs [No. 198 ($P2_13$), No. 212 ($P4_332$), and No. 213 ($P4_132$)] belong to PG T or O [26,52,65] and own a three-dimensional (3D) SVIR at the Γ point. This indicates that single-pair CWFs with a C-2 DP and a SWP can only occur in the three SGs above. The symmetry requirements are listed in Table I and the low-energy effective $\mathbf{k} \cdot \mathbf{p}$ models for the Γ and R points are applied to prove the SWP and C-2 DP (see more details in the Supplemental Material (SM) [66]). Here, three bands of the SWP have the chiral charges of +2, 0, and -2, respectively [see Fig. 1(a)], which corresponds to the chiral pseudospin-1 fermions [1]. The C-2 DP can be represented as the direct sum of two WPs with the same chiral charges of $C = \pm 1$ [Fig. 1(b)], which then contributes to the DP with the double charge. Additionally, in this way, we list all of the single-pair CWFs in spinless systems (see Table SV in the SM [66]).

Here, SGs 212 and 213 are the mirror enantiomers of each other, which are energy degenerate. Thus, in the main text, we only consider a four-band minimal lattice model with SG 212. Its symmetry operators include two twofold screw symmetries ($\tilde{C}_{2x} = \{C_{2x} | \frac{1}{2} \frac{1}{2} 0\}$ and $\tilde{C}_{2y} = \{C_{2y} | 0 \frac{1}{2} \frac{1}{2}\}$), a threefold rotational symmetry $C_{3,111}^+$ along the [111] direction, a fourfold screw symmetry $\tilde{C}_{4z}^+ = \{C_{4z}^+ | \frac{3}{4} \frac{3}{4} \frac{3}{4}\}$, and \mathcal{T} symmetry. Here, based on the band representations [67–69], we select the $4a$ ($\{\frac{1}{8}, \frac{1}{8}, \frac{1}{8}\}$) Wyckoff position occupied by the s orbital to construct this lattice model, as shown in Fig. 2(a). It has

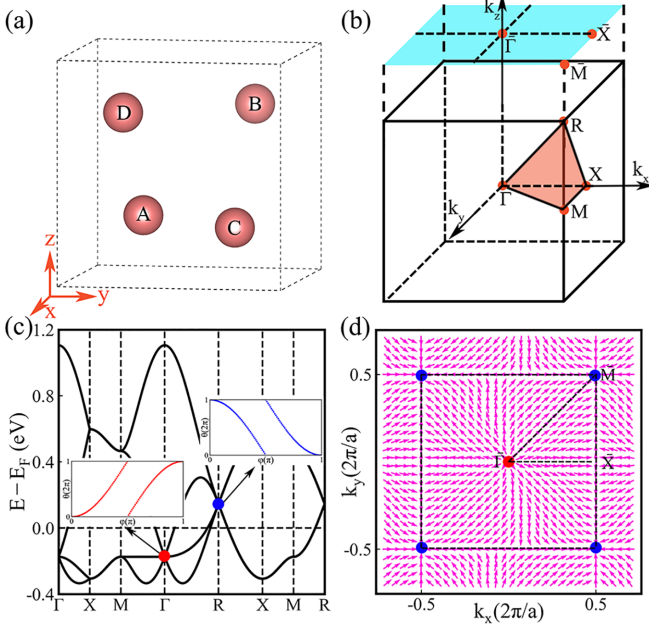


FIG. 2. The four-band minimal lattice model for SG 212. (a) The lattice structure of the 4a ($\{\frac{1}{8}, \frac{1}{8}, \frac{1}{8}\}$) Wyckoff position. (b) The bulk BZ and projected on the (001) surface BZ. (c) The bulk band structure of hopping parameters: $t_0 = 0.145$ and $t_1 = 0.160$. Here, the unit of energy is in eV. The left and right insets represent the WCCs for the SWP and C-2 DP at the Γ and R points, where $\varphi \in [0, \pi]$ is the polar angle, and $\theta \in [0, 2\pi]$ corresponds to the evolution of the WCCs. The red and blue dots indicate the positive and negative chiral charges. (d) The Berry curvature distributions on the (001) surface BZ. The SWP with $C = +2$ as the “source” flows into the “sink” generated by the C-2 DP with $C = -2$.

the four equivalent positions $\{\{\frac{1}{8}, \frac{1}{8}, \frac{1}{8}\}, \{\frac{3}{8}, \frac{7}{8}, \frac{5}{8}\}, \{\frac{7}{8}, \frac{5}{8}, \frac{3}{8}\}, \{\frac{5}{8}, \frac{3}{8}, \frac{7}{8}\}\}$, denoted by A, B, C, and D, respectively. Under the basis $\{\Phi_A(r), \Phi_B(r), \Phi_C(r), \Phi_D(r)\}$, the matrix representations of the symmetry operators are

$$\begin{aligned}
 D(\tilde{C}_{2x}) &= \Gamma_{11}, & D(\tilde{C}_{2y}) &= \Gamma_{10}, & D(T) &= \Gamma_{00}\mathcal{K}, \\
 D(C_{3,111}^+) &= \begin{bmatrix} 1 & 0 & 0 & 0 \\ 0 & 0 & 0 & 1 \\ 0 & 1 & 0 & 0 \\ 0 & 0 & 1 & 0 \end{bmatrix}, \\
 D(\tilde{C}_{4z}^+) &= \begin{bmatrix} 0 & 0 & 0 & 1 \\ 0 & 0 & 1 & 0 \\ 1 & 0 & 0 & 0 \\ 0 & 1 & 0 & 0 \end{bmatrix}, \tag{1}
 \end{aligned}$$

where $\Gamma_{ij} = \sigma_i \otimes \tau_j$ ($i, j = 0, 1, 2, 3$), $\sigma(\tau)_0$ is a 2×2 identity matrix, $\sigma(\tau)_i$ is a Pauli matrix, and \mathcal{K} is the complex conjugate operator. The Hamiltonian is restricted by these symmetries

$$D(\mathcal{O})\mathcal{H}(\mathbf{k})D^{-1}(\mathcal{O}) = \mathcal{H}(\mathcal{O}\mathbf{k}), \tag{2}$$

where \mathcal{O} stands for symmetry operators and it runs over all operators, and $D(\mathcal{O})$ is its matrix representation. Therefore, based on Eqs. (1) and (2), the effective lattice model with SG

212 in the spinless case reads [70,71]

$$\mathcal{H}(\mathbf{k}) = t_0\Gamma_{00} + 2t_1 \begin{bmatrix} 0 & h_{12} & h_{13} & h_{14} \\ h_{12}^* & 0 & h_{23} & h_{24} \\ h_{13}^* & h_{23}^* & 0 & h_{34} \\ h_{14}^* & h_{24}^* & h_{34}^* & 0 \end{bmatrix}. \tag{3}$$

The matrix elements are listed as follows:

$$\begin{aligned}
 h_{12} &= \cos \frac{k_x}{2} \left(\cos \frac{k_y - k_z}{4} + i \sin \frac{k_y - k_z}{4} \right), \\
 h_{13} &= \cos \frac{k_y}{2} \left(\cos \frac{k_x - k_z}{4} + i \sin \frac{k_x - k_z}{4} \right), \\
 h_{14} &= \cos \frac{k_z}{2} \left(\cos \frac{k_x - k_y}{4} + i \sin \frac{k_x - k_y}{4} \right), \\
 h_{23} &= \cos \frac{k_z}{2} \left(\cos \frac{k_x + k_y}{4} + i \sin \frac{k_x + k_y}{4} \right), \\
 h_{24} &= \cos \frac{k_y}{2} \left(\cos \frac{k_x + k_z}{4} + i \sin \frac{k_x + k_z}{4} \right), \\
 h_{34} &= \cos \frac{k_x}{2} \left(\cos \frac{k_y + k_z}{4} + i \sin \frac{k_y + k_z}{4} \right). \tag{4}
 \end{aligned}$$

Here, t_i ($i = 0, 1$) denotes the hopping strength of considered couplings and is a real parameter. The topological properties of these WPs at the Γ and R points are extremely stable and exhibit necessary degeneracy. Thus, we can randomly select these hopping parameters within a reasonable range and ensure that it occurs as a natural result. In Eq. (3), we adopt $t_0 = 0.145$ and $t_1 = 0.160$ in the unit of eV. The four-band minimal lattice model for SG 198 is provided in the SM [66].

The corresponding bulk BZ of the lattice structure of the lattice model is shown in Fig. 2(b), where the cyan square represents the BZ projections in the (001) plane. The associated HSPs are also marked. Based on the hopping parameters above, we calculate the band dispersion along the high-symmetry lines (HSLs), as depicted in Fig. 2(c), where a single pair of WPs do occur at the Γ and R points (highlighted the red and blue dots). They have threefold and fourfold degeneracies with the linear dispersion, respectively. Then, to confirm the chiral charge of these WPs, we calculate the Wannier charge centers (WCCs) by using the Wilson-loop method [72]. We can observe that the threefold degenerate WP at Γ possesses the chiral charge of $C = +2$ [see the left panel of Fig. 2(c)], and the chiral charge of the fourfold degenerate WP is $C = -2$ at the R point, as shown in the right panel of Fig. 2(c). This implies a SWP appears at Γ and a C-2 DP at R. The total chiral charges are zero, which obeys the no-go theorem [63,64]. Besides, the Berry curvature distribution of the (001) plane shows that there is only one “source” at Γ and one “sink” at \bar{R} , and the SWP as the “source” flows into the “sink” generated by the C-2 DP [Fig. 2(d)]. This is consistent with the associated chiral charges. These verify that the Hamiltonian can well describe the band topology of this kind of Weyl semimetal.

The symmetry-guaranteed SWP and C-2 DP with opposite chiral charges can lead to unique nontrivial surface arcs due to the bulk-boundary correspondence. To confirm the topological signatures of the SWP and C-2 DP, we further calculate the

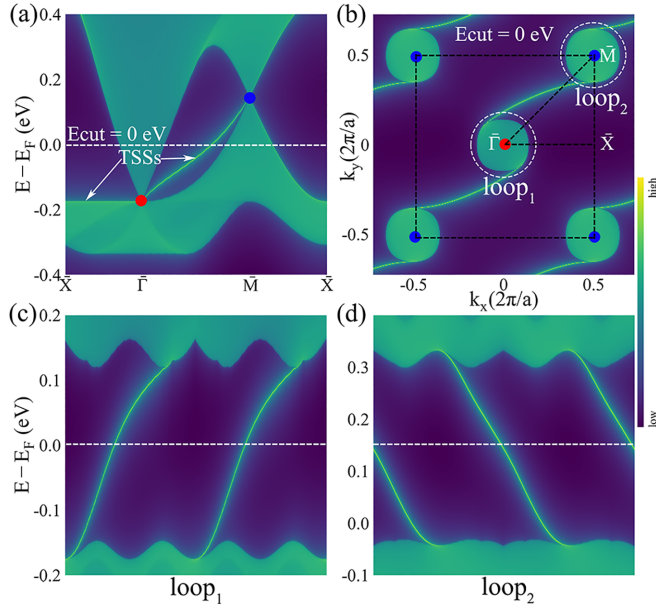


FIG. 3. The TSSs and Fermi arcs of the four-band lattice model for SG 212. (a) The LDOS along $\bar{X}\text{-}\bar{\Gamma}\text{-}\bar{M}\text{-}\bar{X}$ paths on the (001) surface BZ. The white dashed line represents the isoenergy contour $E_{\text{cut}} = 0$ eV. (b) The Fermi arcs at $E_{\text{cut}} = 0$ eV and the associated WPs with the red and blue dots. The double-helical surface arcs occur at $\bar{\Gamma}$ and \bar{M} , respectively. (c) and (d) The surface LDOSs along the two white clockwise loops (loop₁ and loop₂) centered at $\bar{\Gamma}$ and \bar{M} in (b). The white dashed lines are the reference lines.

local density of states (LDOSs) and Fermi arcs by employing the iterative Green's function method [73,74]. According to crystal symmetry, (100), (010), and (001) surfaces are identical and support the same surface states. We here adopt a semi-infinite (001) surface. The Γ and R points are projected to $\bar{\Gamma}$ and \bar{M} on the (001) surface BZ. As illustrated in Fig. 3(a), two TSSs wind around the projected SWP and C-2 DP at $\bar{\Gamma}$ and \bar{M} [see white arrows]. In Fig. 3(b), at the isoenergy contour $E_{\text{cut}} = 0$ eV, the two Fermi arcs wind clockwise around the $\bar{\Gamma}$ point, while the two Fermi arcs wind anticlockwise around the \bar{M} point. This forms the double arc-shaped surface states that originate from the projection of the SWP and C-2 DP. In addition, it can find that two surface arcs are observed to link the projected SWP and C-2 DP because there is only a pair of WPs over the whole BZ, unlike the conventional WPs with opposite chiral charges exhibiting internally linked performance. This is consistent with the Berry curvature distribution. Moreover, to visualize the helicoidal surface states, we calculate the surface LDOSs along two clockwise loops (loop₁ and loop₂) centered at $\bar{\Gamma}$ and \bar{M} [see Figs. 3(c) and 3(d)]. For the loop₁, two right-moving chiral edge modes appear inside the band gap. But loop₂ encompasses the two left-moving chiral edge modes. This also hints that they have opposite chirality with $C = \pm 2$.

III. MATERIAL REALIZATION WITH ABUNDANT REAL CANDIDATES

Symmetry arguments, low-energy effective models, and the minimal lattice models provide a fundamental theoretical

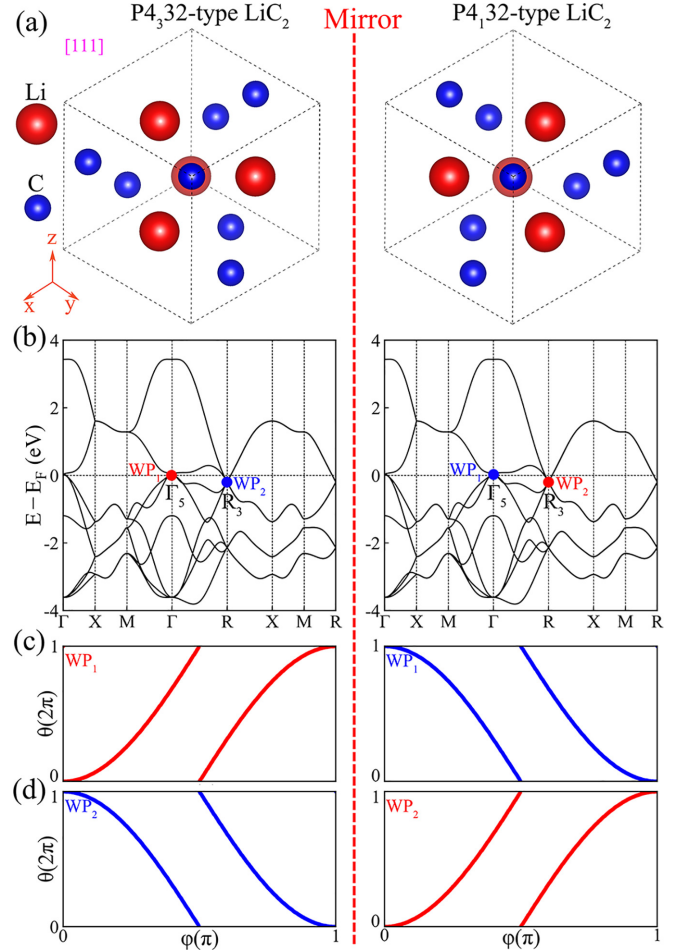


FIG. 4. The representative materials for a single pair of WPs with opposite chiral charges of $C = \pm 2$. (a) The views of the two enantiomers along the [111] direction, which are connected by the mirror symmetry. (b) The bulk band structures along the HSLs and the relevant SVIRs with the corresponding SGs P4₃32 and P4₁32. The band crossings near the Fermi level are marked WP₁ and WP₂, respectively. (c) and (d) The evolutions of WCCs for WP₁ and WP₂, respectively. The WPs of the two enantiomers are characterized by opposite chiral charges.

strategy to investigate a single pair of WPs with the coexistence of the SWP and C-2 DP. Herein, by first-principles calculations, we take the realistic crystal material P4₃32-type LiC₂ and its mirror enantiomer P4₁32-type LiC₂, which are connected by the mirror symmetry [Fig. 4(a)], as examples to confirm the chiral fermions with $C = \pm 2$. The other material candidates are summarized in the SM [66]. Top and side views of the crystal structure of P4₃32-type LiC₂ are shown in Fig. S2 in the SM [66], which crystallizes in a chiral cubic lattice with SG P4₃32. Each unit cell contains four Li and twelve C atoms, occupying the $4a$ ($\frac{1}{8}, \frac{1}{8}, \frac{1}{8}$) and $8c$ (0.405, 0.405, 0.405) Wyckoff positions, denoted by red and blue balls, respectively. Its enantiomer with SG P4₁32 is displayed in Fig. S2 in the SM [66], in which the Li and C atoms occupy two Wyckoff positions: $4a$ ($\frac{7}{8}, \frac{7}{8}, \frac{7}{8}$) and $8c$ (0.595, 0.595, 0.595). Their optimized lattice parameter is $|\mathbf{a}| = 4.31$ Å. They are mechanically, thermodynamically, and dynamically stable, based on the results of the elastic

TABLE II. The corresponding energies, locations, and chiral charges of the inequivalent WPs in two types of LiC_2 with different SGs.

SG	WP	$E - E_F$ (meV)	Location	Charge
P4 ₃ 32	WP ₁	31.29	Γ	+2
	WP ₂	-202.11	R	-2
P4 ₁ 32	WP ₁	31.29	Γ	-2
	WP ₂	-202.11	R	+2

constants, the density-functional-base *ab initio* molecular dynamics simulations, and the phonon dispersion along the HSLs (see Fig. S3 in the SM [66]).

We next discuss the electronic properties of two enantiomers. Since the Li atom is lighter than the C atom, they both are ideal spinless systems with the negligible SOC effect, as shown in Fig. S3 in the SM [66]. Hence, we only consider their band structures without SOC and mark the relevant SVIRs [Fig. 4(b)]. The related symbols of SVIRs are listed in Tables SIII and SIV in the SM [66]. We note that the two enantiomers are indeed energy degenerate due to the mirror symmetry. Besides, one shows clearly that the threefold degenerate WP₁ (SWP) with a 3D SVIR Γ_5 is located at Γ and the fourfold degenerate WP₂ (C-2 DP) with a 4D SVIR R_3 , different from P2₁3-type crystals with two 2D SVIRs, is at the R point [75]. By carefully screening energy differences between the lowest conduction and the highest valence bands, we find only one pair of WPs in the whole BZ and verify the absence of any additional quasiparticles. This is consistent with the symmetry analysis and the lattice model. Then, to examine the chiral charges of different types of WPs, we employ the tight-binding Hamiltonian based on the maximally localized Wannier functions [76,77] to calculate the WCCs by using the Wilson-loop method [72]. As shown in Figs. 4(c) and 4(d), the evolutions of WCCs of P4₃32-type LiC_2 show that the WPs (SWP and C-2 DP) possess the chiral charges of +2 and -2, respectively. On the contrary, since Berry curvature is an axial tensor, its enantiomer P4₁32-type LiC_2 has the chiral charges of -2 and +2 at Γ and R, respectively. This indicates that the chirality of chiral fermions can be reversed by altering the structural chirality, establishing a mapping between fermionic chirality and structural chirality. The detailed information, including the corresponding energies, locations, and chiral charges, is listed in Table II. Moreover, it can find the SWP and C-2 DP, near the Fermi level, which can be viewed as ideal chiral fermions due to the ultraclean band dispersions.

To respect the chiral charges of the SWP and C-2 DP in the two enantiomers, we further calculate the LDOS and projected Fermi arcs by employing the WANNIERTOOLS package [78]. The LDOSs of the semi-infinite (001) surface of the two enantiomers are displayed in Fig. 5(a). Two visible TSSs link the projected SWP and C-2 DP surrounding the projection points $\bar{\Gamma}$ and \bar{M} . The alternating connection between starting and ending points leads to the Fermi arc traversing the entire BZ. The isoenergy contour of the (001) surface at $E_{\text{cut}} = -0.1$ eV provides the ultralong surface arcs in Fig. 5(b). We can see that the Fermi arcs of two enantiomers possess the reversal of Fermi-arc connections. Furthermore, we visualize the helicoidal (or double arc-shaped) surface arcs by calculating the

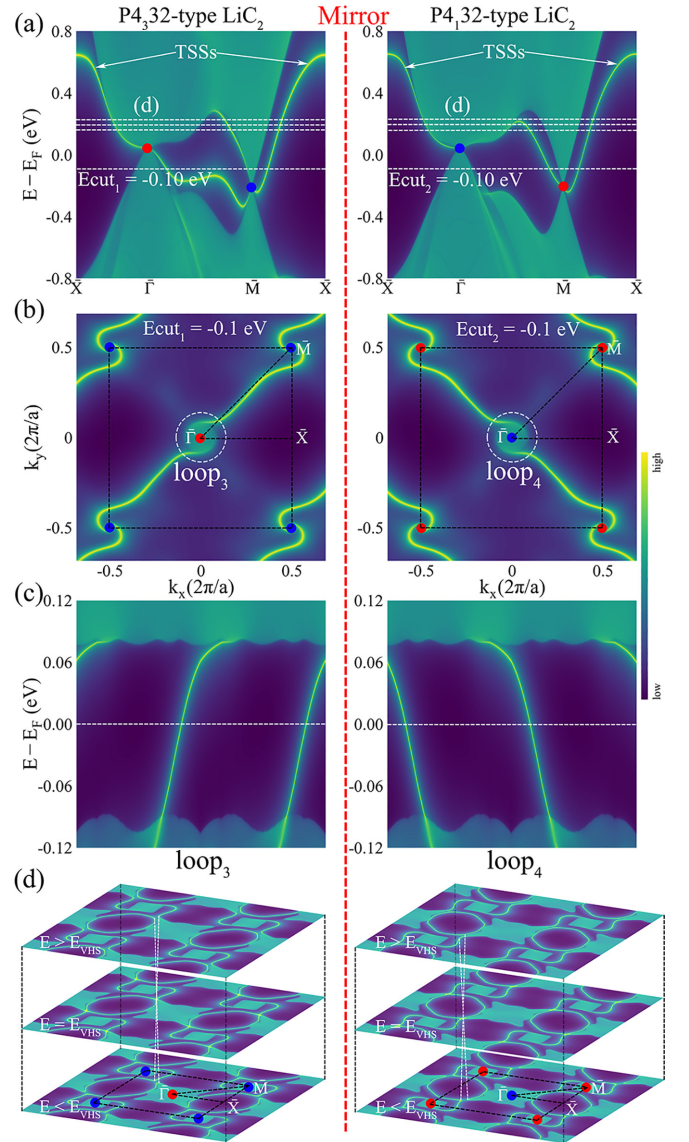


FIG. 5. (a) The LDOSs of the two enantiomers along $\bar{X}-\bar{\Gamma}-\bar{M}-\bar{X}$ paths on the (001) surface BZ. The white dashed line represents different isoenergy contours. (b) Their Fermi arcs at $E_{\text{cut}} = -0.1$ eV and positions of the WPs. The double-helicoid surface arcs occur at $\bar{\Gamma}$ and \bar{M} , respectively. (c) The surface LDOSs along the two white clockwise loops (loop₃ and loop₄) centered at $\bar{\Gamma}$ in (b). Two right-moving and left-moving chiral double-helicoid TSSs occur naturally. (d) Three isoenergy contours at three energies (0.20, 0.215, and 0.23 eV) indicated by three horizontal dashed lines in (a). Lifshitz transitions occur in the evolutions of their surface arc with the opposite position.

surface LDOSs along two white clockwise loops (loop₃ and loop₄) centered at $\bar{\Gamma}$. It appears as two right-moving chiral edge modes around $\bar{\Gamma}$ in P4₃32-type LiC_2 [see the left panel of Fig. 5(c)]. As expected, owing to the mirror symmetry, the opposite situation is observed in its mirror enantiomer, as shown in the right panel of Fig. 5(c). Besides, the evolutions of their surface arcs are illustrated by three isoenergy contours [Fig. 5(d)], in which the surface arcs are visualized and type-II VHSSs occur clearly in the arclike surface states with the opposite position. Since the R and Γ points have opposite chiral

charges, the helicoid arcs wind in opposite directions around \bar{M} and $\bar{\Gamma}$ with increasing energies. Moreover, the nonuniform winding speeds cause the Fermi arcs to touch at a generic momentum \mathbf{k} between $\bar{\Gamma}$ and \bar{M} to form a type-II intrahelicoid arc VHS. Such VHSs indicate electronic instability and may result in electronic correlations [79]. All topological properties of the two enantiomers are consistent with our minimal lattice model. It is worth noting that they both host the ultralong Fermi arcs spanning the entire BZ, and their TSSs are not covered by the bulk band projection, which provides great promise for experimental detection and further applications.

IV. SUMMARY

In summary, based on symmetry arguments, low-energy effective models, and the minimal lattice model, we prove that the single-pair high-fold CWFs with $C = \pm 2$ can occur in chiral cubic crystals. Then, by first-principles calculations, we take the two enantiomers (P₄32-type LiC₂ and P₄132-

type LiC₂) with high thermal stability as ideal examples to confirm it. They do appear as ultralong visible double-helicoid Fermi arcs on the (001) surface BZ and own the reversal of Fermi-arc connections. The type-II VHSs on the (001) surface of P₄132-type LiC₂ make it possible to promise an excellent playground for further observations of interaction-driven order states, such as the chirality-locked CDW, and superconductivity [45,46]. Besides, the CWFs also carry a monopolelike orbital-momentum locking texture, which may lead to the large orbital Hall effect and the giant chirality-locked orbital magnetoelectric effect [80].

ACKNOWLEDGEMENTS

This work was supported by the National Natural Science Foundation of China (NSFC, Grants No. 12174040, No. 12204074, No. 12222402, and No. 12347101), the China National Postdoctoral Program for Innovative Talent (Grant No. BX20220367), and Chongqing Natural Science Foundation (Grant No. cstc2020jcyj-msxmX0118).

-
- [1] B. Bradlyn, J. Cano, Z. Wang, M. G. Vergniory, C. Felser, R. J. Cava, and B. A. Bernevig, *Science* **353**, aaf5037 (2016).
- [2] S.-M. Huang, S.-Y. Xu, I. Belopolski, C.-C. Lee, G. Chang, T.-R. Chang, B. Wang, N. Alidoust, G. Bian, M. Neupane, D. Sanchez, H. Zheng, H.-T. Jeng, A. Bansil, T. Neupert, H. Lin, and M. Z. Hasan, *Proc. Natl. Acad. Sci. USA* **113**, 1180 (2016).
- [3] B. J. Wieder, Y. Kim, A. M. Rappe, and C. L. Kane, *Phys. Rev. Lett.* **116**, 186402 (2016).
- [4] A. Bouhon and A. M. Black-Schaffer, *Phys. Rev. B* **95**, 241101(R) (2017).
- [5] M. Z. Hasan, G. Chang, I. Belopolski, G. Bian, S.-Y. Xu, and J.-X. Yin, *Nat. Rev. Mater.* **6**, 784 (2021).
- [6] Z.-M. Yu, Z. Zhang, G.-B. Liu, W. Wu, X.-P. Li, R.-W. Zhang, S. A. Yang, and Y. Yao, *Sci. Bull.* **67**, 375 (2022).
- [7] C. Fang, M. J. Gilbert, X. Dai, and B. A. Bernevig, *Phys. Rev. Lett.* **108**, 266802 (2012).
- [8] S. S. Tsirkin, I. Souza, and D. Vanderbilt, *Phys. Rev. B* **96**, 045102 (2017).
- [9] Y. J. Jin, Y. Xu, Z. J. Chen, and H. Xu, *Phys. Rev. B* **105**, 035141 (2022).
- [10] T. Zhang, R. Takahashi, C. Fang, and S. Murakami, *Phys. Rev. B* **102**, 125148 (2020).
- [11] W. Wu, Z.-M. Yu, X. Zhou, Y. X. Zhao, and S. A. Yang, *Phys. Rev. B* **101**, 205134 (2020).
- [12] C. Cui, X.-P. Li, D.-S. Ma, Z.-M. Yu, and Y. Yao, *Phys. Rev. B* **104**, 075115 (2021).
- [13] X. Xiao, Y. Jin, D.-S. Ma, W. Kong, J. Fan, R. Wang, and X. Wu, *Phys. Rev. B* **108**, 075130 (2023).
- [14] X. Feng, W. Wu, Y. Huang, Z.-M. Yu, and S. A. Yang, *Phys. Rev. B* **104**, 115116 (2021).
- [15] D. Wang, C. Cui, X.-P. Li, and R.-W. Zhang, *Phys. Rev. B* **107**, 195125 (2023).
- [16] H. D. Flack, *Helv. Chim. Acta* **86**, 905 (2003).
- [17] P. Tang, Q. Zhou, and S.-C. Zhang, *Phys. Rev. Lett.* **119**, 206402 (2017).
- [18] D. Rees, K. Manna, B. Lu, T. Morimoto, H. Borrmann, C. Felser, J. E. Moore, D. H. Torchinsky, and J. Orenstein, *Sci. Adv.* **6**, eaba0509 (2020).
- [19] G. Chang, S.-Y. Xu, B. J. Wieder, D. S. Sanchez, S.-M. Huang, I. Belopolski, T.-R. Chang, S. Zhang, A. Bansil, H. Lin, and M. Z. Hasan, *Phys. Rev. Lett.* **119**, 206401 (2017).
- [20] D. Takane, Z. Wang, S. Souma, K. Nakayama, T. Nakamura, H. Oinuma, Y. Nakata, H. Iwasawa, C. Cacho, T. Kim, K. Horiba, H. Kumigashira, T. Takahashi, Y. Ando, and T. Sato, *Phys. Rev. Lett.* **122**, 076402 (2019).
- [21] Z. Rao, H. Li, T. Zhang, S. Tian, C. Li, B. Fu, C. Tang, L. Wang, Z. Li, W. Fan, J. Li, Y. Huang, Z. Liu, Y. Long, C. Fang, H. Weng, Y. Shi, H. Lei, Y. Sun, T. Qian, and H. Ding, *Nature (London)* **567**, 496 (2019).
- [22] D. S. Sanchez, I. Belopolski, T. A. Cochran, X. Xu, J.-X. Yin, G. Chang, W. Xie, K. Manna, V. Süß, C.-Y. Huang, N. Alidoust, D. Multer, S. S. Zhang, N. Shumiya, X. Wang, G.-Q. Wang, T.-R. Chang, C. Felser, S.-Y. Xu, S. Jia, H. Lin, and M. Z. Hasan, *Nature (London)* **567**, 500 (2019).
- [23] N. B. M. Schröter, D. Pei, M. G. Vergniory, Y. Sun, K. Manna, F. de Juan, J. A. Krieger, V. Süß, M. Schmidt, P. Dudin, B. Bradlyn, T. K. Kim, T. Schmitt, C. Cacho, C. Felser, V. N. Strocov, and Y. Chen, *Nat. Phys.* **15**, 759 (2019).
- [24] E. J. König, H.-Y. Xie, D. A. Pesin, and A. Levchenko, *Phys. Rev. B* **96**, 075123 (2017).
- [25] F. de Juan, A. G. Grushin, T. Morimoto, and J. E. Moore, *Nat. Commun.* **8**, 15995 (2017).
- [26] F. Flicker, F. de Juan, B. Bradlyn, T. Morimoto, M. G. Vergniory, and A. G. Grushin, *Phys. Rev. B* **98**, 155145 (2018).
- [27] H. Nielsen and M. Ninomiya, *Phys. Lett. B* **130**, 389 (1983).
- [28] H.-J. Kim, K.-S. Kim, J.-F. Wang, M. Sasaki, N. Satoh, A. Ohnishi, M. Kitaura, M. Yang, and L. Li, *Phys. Rev. Lett.* **111**, 246603 (2013).
- [29] Z.-M. Yu, Y. Yao, and S. A. Yang, *Phys. Rev. Lett.* **117**, 077202 (2016).
- [30] Y. X. Zhao and S. A. Yang, *Phys. Rev. Lett.* **126**, 046401 (2021).
- [31] X. Wang, F. Zhou, Z. Zhang, W. Wu, Z.-M. Yu, and S. A. Yang, *Phys. Rev. B* **106**, 195129 (2022).
- [32] G. Ding, C. Xie, J. Bai, Z. Cheng, X. Wang, and W. Wu, *Phys. Rev. B* **108**, L020302 (2023).

- [33] G. Ding, J. Wang, Z.-M. Yu, Z. Zhang, W. Wang, and X. Wang, *Phys. Rev. Mater.* **7**, 014202 (2023).
- [34] Z.-Q. Wang, Q.-B. Liu, X.-F. Yang, and H.-H. Fu, *Phys. Rev. B* **106**, L161302 (2022).
- [35] Q. Chen, F. Chen, Y. Pan, C. Cui, Q. Yan, L. Zhang, Z. Gao, S. A. Yang, Z.-M. Yu, H. Chen, B. Zhang, and Y. Yang, *Nat. Commun.* **13**, 7359 (2022).
- [36] Y. Yang, C. Xie, Y. Cui, X. Wang, and W. Wu, *Phys. Rev. B* **107**, 054310 (2023).
- [37] X.-P. Li, D. Zhou, Y. Wu, Z.-M. Yu, F. Li, and Y. Yao, *Phys. Rev. B* **106**, L220302 (2022).
- [38] P. Wu, G. Liu, X. Hu, and H. Xu, *Phys. Rev. B* **108**, 054305 (2023).
- [39] M. Yao, K. Manna, Q. Yang, A. Fedorov, V. Voroshnin, B. V. Schwarze, J. Hornung, S. Chattopadhyay, Z. Sun, S. N. Guin, J. Wosnitza, H. Borrmann, C. Shekhar, N. Kumar, J. Fink, Y. Sun, and C. Felser, *Nat. Commun.* **11**, 2033 (2020).
- [40] N. B. M. Schroter, S. Stolz, K. Manna, F. de Juan, M. G. Vergniory, J. A. Krieger, D. Pei, T. Schmitt, P. Dudin, T. K. Kim, C. Cacho, B. Bradlyn, H. Borrmann, M. Schmidt, R. Widmer, V. N. Strocov, and C. Felser, *Science* **369**, 179 (2020).
- [41] B. Q. Lv, Z.-L. Feng, J.-Z. Zhao, N. F. Q. Yuan, A. Zong, K. F. Luo, R. Yu, Y.-B. Huang, V. N. Strocov, A. Chikina, A. A. Soluyanov, N. Gedik, Y.-G. Shi, T. Qian, and H. Ding, *Phys. Rev. B* **99**, 241104(R) (2019).
- [42] D. S. Sanchez, T. A. Cochran, I. Belopolski, Z.-J. Cheng, X. P. Yang, Y. Liu, T. Hou, X. Xu, K. Manna, C. Shekhar *et al.*, *Nat. Phys.* **19**, 682 (2023).
- [43] G. Li, H. Yang, P. Jiang, C. Wang, Q. Cheng, S. Tian, G. Han, C. Shen, X. Lin, H. Lei *et al.*, *Nat. Commun.* **13**, 2914 (2022).
- [44] Z. Rao, Q. Hu, S. Tian, Q. Qu, C. Chen, S. Gao, Z. Yuan, C. Tang, W. Fan, J. Huang *et al.*, *Sci. Bull.* **68**, 165 (2023).
- [45] H. Yao and F. Yang, *Phys. Rev. B* **92**, 035132 (2015).
- [46] Y.-X. Li and X.-T. Yang, *Front. Phys.* **16**, 53501 (2021).
- [47] L.-H. Hu, C. Guo, Y. Sun, C. Felser, L. Elcoro, P. J. W. Moll, C.-X. Liu, and B. A. Bernevig, *Phys. Rev. B* **107**, 125145 (2023).
- [48] C. K. Barman, C. Mondal, S. Pujari, B. Pathak, and A. Alam, *Phys. Rev. B* **102**, 155147 (2020).
- [49] T. Zhang, Z. Song, A. Alexandradinata, H. Weng, C. Fang, L. Lu, and Z. Fang, *Phys. Rev. Lett.* **120**, 016401 (2018).
- [50] H. Miao, T. T. Zhang, L. Wang, D. Meyers, A. H. Said, Y. L. Wang, Y. G. Shi, H. M. Weng, Z. Fang, and M. P. M. Dean, *Phys. Rev. Lett.* **121**, 035302 (2018).
- [51] Y. Yang, H.-x. Sun, J.-p. Xia, H. Xue, Z. Gao, Y. Ge, D. Jia, S.-q. Yuan, Y. Chong, and B. Zhang, *Nat. Phys.* **15**, 645 (2019).
- [52] Y. J. Jin, Z. J. Chen, X. L. Xiao, and H. Xu, *Phys. Rev. B* **103**, 104101 (2021).
- [53] X.-Y. Kang, J.-Y. Li, and S. Li, *Phys. Rev. B* **108**, 125127 (2023).
- [54] K. S. Novoselov, A. K. Geim, S. V. Morozov, D. Jiang, M. I. Katsnelson, I. V. Grigorieva, S. V. Dubonos, and A. A. Firsov, *Nature (London)* **438**, 197 (2005).
- [55] C. Zhang, X.-Y. Ding, L.-Y. Gan, Y. Cao, B.-S. Li, X. Wu, and R. Wang, *Phys. Rev. B* **101**, 235119 (2020).
- [56] J. Wei, W. Kong, X. Xiao, R. Wang, L.-Y. Gan, J. Fan, and X. Wu, *J. Phys. Chem. Lett.* **13**, 5508 (2022).
- [57] W. Kong, R. Wang, X. Xiao, F. Zhan, L.-Y. Gan, J. Wei, J. Fan, and X. Wu, *J. Phys. Chem. Lett.* **12**, 10874 (2021).
- [58] W. Wu, Y. Xie, and Y. Chen, *Phys. Rev. Mater.* **5**, 104201 (2021).
- [59] T. Deng, B. Zheng, F. Zhan, J. Fan, X. Wu, and R. Wang, *Phys. Rev. B* **102**, 201105(R) (2020).
- [60] H. Weng, Y. Liang, Q. Xu, R. Yu, Z. Fang, X. Dai, and Y. Kawazoe, *Phys. Rev. B* **92**, 045108 (2015).
- [61] J. Zhang, R. Wang, X. Zhu, A. Pan, C. Han, X. Li, D. Zhao, C. Ma, W. Wang, H. Su, and C. Niu, *Nat. Commun.* **8**, 683 (2017).
- [62] X.-W. Yi, Z. Zhang, Z.-W. Liao, X.-J. Dong, J.-Y. You, and G. Su, *Nano Today* **42**, 101346 (2022).
- [63] H. Nielsen and M. Ninomiya, *Nucl. Phys. B* **185**, 20 (1981).
- [64] H. Nielsen and M. Ninomiya, *Nucl. Phys. B* **193**, 173 (1981).
- [65] C. J. Bradley and A. P. Cracknell, *Acta Cryst. A* **29**, 581 (1973).
- [66] See Supplemental Material at <http://link.aps.org/supplemental/10.1103/PhysRevB.109.165136> for character tables of the point/little group; low-energy effective $\mathbf{k} \cdot \mathbf{p}$ models of the Γ and R points for SGs $P2_13$, $P4_332$, and $P4_132$; the four-band minimal lattice model for SG $P2_13$; detailed computational methods of first-principles calculations, SVIRs of the point/little group; phonon dispersions; bulk band structures with/without SOC; and the LDOSs and Fermi arcs of crystal structure on the (001) surfaces BZ of the candidate materials ($P4_132$ -type LiC_2 , $P4_132$ -type NaC_2 , and $P2_13$ -type BeN), which includes Refs. [1,63–65,70–78,81–91].
- [67] J. Zak, *Phys. Rev. Lett.* **45**, 1025 (1980).
- [68] J. Zak, *Phys. Rev. B* **23**, 2824 (1981).
- [69] J. Zak, *Phys. Rev. B* **26**, 3010 (1982).
- [70] P. H. Jacobse, *Comput. Phys. Commun.* **244**, 392 (2019).
- [71] Z. Zhang, Z.-M. Yu, G.-B. Liu, and Y. Yao, *Comput. Phys. Commun.* **270**, 108153 (2022).
- [72] R. Yu, X. L. Qi, A. Bernevig, Z. Fang, and X. Dai, *Phys. Rev. B* **84**, 075119 (2011).
- [73] M. P. L. Sancho, J. M. L. Sancho, and J. Rubio, *J. Phys. F* **14**, 1205 (1984).
- [74] M. P. L. Sancho, J. M. L. Sancho, J. M. L. Sancho, and J. Rubio, *J. Phys. F* **15**, 851 (1985).
- [75] J. Gao, Q. Wu, C. Persson, and Z. Wang, *Comput. Phys. Commun.* **261**, 107760 (2021).
- [76] N. Marzari and D. Vanderbilt, *Phys. Rev. B* **56**, 12847 (1997).
- [77] A. A. Mostofi, J. R. Yates, Y.-S. Lee, I. Souza, D. Vanderbilt, and N. Marzari, *Comput. Phys. Commun.* **178**, 685 (2008).
- [78] Q. Wu, S. Zhang, H.-F. Song, M. Troyer, and A. A. Soluyanov, *Comput. Phys. Commun.* **224**, 405 (2018).
- [79] S.-W. Kim, H. Oh, E.-G. Moon, and Y. Kim, *Nat. Commun.* **14**, 591 (2023).
- [80] Q. Yang, J. Xiao, I. Robredo, M. G. Vergniory, B. Yan, and C. Felser, *Proc. Natl. Acad. Sci. USA* **120**, e2305541120 (2023).
- [81] M. Gell-Mann, *Phys. Rev.* **125**, 1067 (1962).
- [82] P. Hohenberg and W. Kohn, *Phys. Rev.* **136**, B864 (1964).
- [83] W. Kohn and L. Sham, *Phys. Rev.* **140**, A1133 (1965).
- [84] G. Kresse and J. Furthmüller, *Comput. Mater. Sci.* **6**, 15 (1996).
- [85] G. Kresse and J. Furthmüller, *Phys. Rev. B* **54**, 11169 (1996).
- [86] P. E. Blöchl, *Phys. Rev. B* **50**, 17953 (1994).
- [87] J. P. Perdew, K. Burke, and M. Ernzerhof, *Phys. Rev. Lett.* **77**, 3865 (1996).
- [88] H. J. Monkhorst and J. D. Pack, *Phys. Rev. B* **13**, 5188 (1976).
- [89] A. Togo, F. Oba, and I. Tanaka, *Phys. Rev. B* **78**, 134106 (2008).
- [90] X. Gonze and C. Lee, *Phys. Rev. B* **55**, 10355 (1997).
- [91] F. Mouhat and F.-X. Coudert, *Phys. Rev. B* **90**, 224104 (2014).